Vacancy-Driven Anisotropic Defect Distribution in the Battery-Cathode Material LiFePO_{4}

Jaekwang Lee, Wu Zhou, Juan C. Idrobo, Stephen J. Pennycook, and Sokrates T. Pantelides

Phys. Rev. Lett. **107**, 085507 — Published 18 August 2011

DOI: 10.1103/PhysRevLett.107.085507

Vacancy-driven anisotropic defect distribution in the novel battery-cathode material $LiFePO_4$

Jaekwang Lee,[1,2] Wu Zhou,[1,2] Juan C. Idrobo,[1,2] Stephen J. Pennycook,[2] and Sokrates T. Pantelides[1,2]

[1]*Department of Physics & Astronomy, Vanderbilt University, Nashville, TN 37235, USA*
[2]*Materials Science & Technology Division, Oak Ridge National Laboratory, Oak Ridge, TN 37831, USA*

Li-ion mobility in $LiFePO_4$, a key property for energy applications, is impeded by Fe antisite defects (Fe_{Li}) that form in select b-axis channels. Here we combine first-principles calculations, statistical mechanics, and scanning transmission electron microscopy (STEM) to identify the origin of the effect: Li vacancies (V_{Li}) are confined in one dimensional b-axis channels, shuttling between neighboring Fe_{Li}. Segregation in select channels results in shorter Fe_{Li}-Fe_{Li} spans, whereby the energy is lowered by the V_{Li}'s spending more time bound to endpoint Fe_{Li}'s. V_{Li}-Fe_{Li}-V_{Li} complexes also form, accounting for observed electron energy loss spectroscopy (EELS) features.

PACS numbers: 82.47.Aa, 61.72.Bb, 68.55.Ln, 61.72.Ff

$LiFePO_4$ is a promising new-generation cathode material for Li rechargeable batteries because of its high energy density, high safety, low cost, and environmental friendliness [1–3]. The Li ion mobility is the key parameter for battery applications with high energy density. Computational and experimental studies of $LiFePO_4$ indicate that Li^+ ion migration occurs preferentially via one dimensional channels oriented along the [010] direction (b-axis) [4]. Such one-dimensional diffusion, however, is highly sensitive to the presence of immobile or low-mobility defects in the diffusion path. Even a single immobile defect in the path can block long-range diffusion.

Recently, Chung *et al*. reported that iron antisite defects (Fe_{Li}) form preferentially in *only a few* channels along the b-axis instead of being homogeneously distributed in the lattice [5]. This kind of segregation is important because only a few diffusion channels are blocked, leaving most of them available for Li diffusion. The ability to control this segregation is, therefore, necessary in order to maximize the fraction of unblocked diffusion channels and optimize device performance. The cause of the Fe_{Li} segregation, however, remains unknown.

In this Letter, we use first-principles calculations and statistical mechanics to show that the observed segregation of Fe_{Li} defects is the result of an unusual energy-lowering mechanism that is a feature of the one-dimensional nature of the Li diffusion paths. To unveil this mechanism, we need to recognize that the b-axis channels are one-dimensional arrays of Li ions and that the presence of V_{Li} is essential for Li migration. An appropriate concentration of V_{Li} is in fact built in during the synthesis of the material. If $LiFePO_4$ were a material where Li diffusion could occur in three dimensions, then the Fe_{Li} defects would be randomly distributed. The one-dimensional nature of Li diffusion induces segregation in only a few channels as follows. When a number of Fe_{Li} are present in a channel, the V_{Li}'s are confined in segments whose length is equal to the Fe_{Li} spacing. V_{Li}'s are then forced to shuttle between neighboring Fe_{Li}'s, but they also spend time being bound to end-point Fe_{Li}'s. Segregation of Fe_{Li}'s along a few b-axis channels decreases the mean distance between Fe_{Li}'s, which then increases the time that the V_{Li} spend bound to end-point Fe_{Li}'s. The net result is a systematic energy lowering that drives the segregation during the synthesis of the material. Based on a one-dimensional random walk with absorbing boundaries, we derive an analytical expression for the total energy lowering E(L) as a function of temperature and the average distance, L, between neighboring Fe_{Li}'s. Finally, we report new atomically-resolved EELS obtained with an aberration-corrected STEM. Analysis of the Fe $L_{2,3}$ edge fine structure reveals that Fe_{Li} in the b-axis channels has a slightly higher oxidation state relative to the nominal value of +2 for Fe in $LiFePO_4$. This effect can be attributed to the formation of V_{Li}-Fe_{Li}-V_{Li} clusters, which is consistent with the energy-lowering mechanism proposed here: a Fe_{Li} in a b-axis channel can bind a V_{Li} on either side for a fraction of time as the V_{Li} shuttle between end-point Fe_{Li}'s.

The calculations were performed using density functional theory (DFT) in the generalized gradient approximation (GGA) and the projector-augmented wave method with a plane-wave basis as implemented in the Vienna ab initio simulation package (VASP) code [6]. We used a kinetic energy cut-off of 500 eV, 1×2×2 supercell (Fig. 1(a)) or 1×3×2 supercell to accommodate larger defect separations, and a 6×6×6 Monkhorst-Pack k-point mesh centered at the Γ-point. We applied a Hubbard U correction with U = 4.3 eV to describe the Fe-3d states. A U_{eff} (U-J) value of 4.3 eV was chosen based on the average values for Fe^{2+} (U_{eff}=3.7 eV in $LiFePO_4$) and Fe^{3+} (U_{eff}=4.9 eV for $FePO_4$) calculated by Zhou *et al*. [7]. Ionic positions were relaxed using a conjugate gradient minimization until all the forces acting on ions were smaller than 40 meV/Å per ion.

We note that prior papers on $LiFePO_4$ and similar compounds often refer to antisite defects as being "cation exchange pairs", e.g., Fe_{Li} and Li_{Fe} pairs, assessing the energy of their formation by the net cation exchange energy

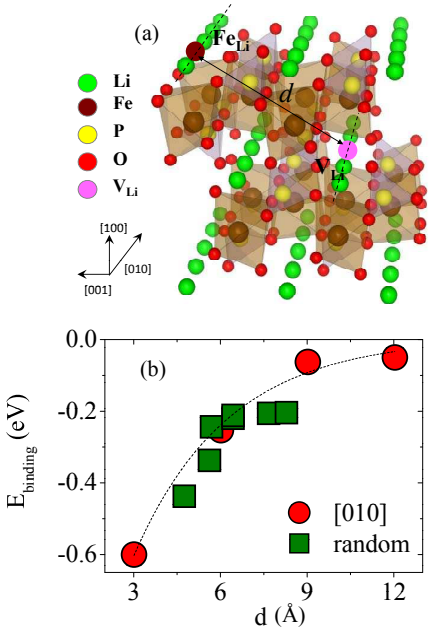

FIG. 1: (Color online) (a) Schematic of $Li_{14}Fe_{17}P_{16}O_{64}$ including one Fe_{Li}-V_{Li} pair separated by a distance d. (b) Binding energy for Fe_{Li}-V_{Li} pairs as a function of separation d. The red points for Fe_{Li} and V_{Li} on the same b-axis, green points for Fe_{Li} and V_{Li} on different b-axes.

(the two defects can be either far from each other or bound in close proximity) [5, 8, 9]. However, the concentrations of Fe_{Li} and Li_{Fe} are in fact independent and, in equilibrium, are governed by the respective formation energies, which depend on the chemical potentials of pertinent species (see, e.g., Ref. [10]). In turn, the chemical potentials depend on the growth conditions, i.e., the nature of the Fe and Li sources (reservoirs). In a similar way, prior papers assign a nominal charge to defects corresponding to the "oxidation state", which is *not* a physical charge [11]. The actual charge states of defects are in fact controlled by the Fermi energy, which in turn is controlled by other means, e.g., doping. Consequently, the formation energies of charged defects are also functions of the electron chemical potential, namely the Fermi energy [10]. Concentrations of defects can of course have non-equilibrium values, controlled by kinetic constraints during growth. In the present work we consider Fe_{Li} defects in $LiFePO_4$, which have been observed by electron microscopy (see Figure 4 and [5, 12]). The presence of Li_{Fe} defects is not relevant to the scope of this paper. Similarly, V_{Li}'s are typically viewed together with Li interstitials as "Frenkel pairs" [8, 9], but the concentrations of the two defects are in fact independent. We will be concerned only with V_{Li}'s, which are known to form during synthesis [8] and are indispensable for Li diffusion.

In order to investigate the effect of V_{Li}'s on the aggregation of Fe_{Li} defects, we calculated the binding energy between a Fe_{Li} in a b-axis channel and a V_{Li} separated by a distance d. The binding energy is defined by $E_b = E_{Fe_{Li}-V_{Li}} - (E_{Fe_{Li}} + E_{V_{Li}})/2$, where $E_{Fe_{Li}-V_{Li}}$, $E_{Fe_{Li}}$ and $E_{V_{Li}}$ are the total energies of supercells containing a Fe_{Li}-V_{Li} bound pair, a Fe_{Li}, and a V_{Li}, respectively. The results are shown in Fig. 1(b). The zero of energy corresponds to infinite separation between the two defects. The red points correspond to the V_{Li} being in the same b-axis channel with the Fe_{Li}. The green points correspond to the V_{Li} being in a different channel. As expected, the largest binding energy, 0.6 eV, is for the nearest-neighbor pair along the b-axis channel ($d \sim 3$ Å). This value is in agreement with previous estimates based on classical potentials [8, 9]. We note that the binding energy displays a Coulombic dependence d^{-1} on the separation distance d, suggesting that the two defects in a neutral supercell carry opposite charges (as noted earlier, the values of these charges are in principle controlled by the Fermi energy, which in turn can be controlled by other means, e.g., doping; the results here indicate that in a neutral, undoped supercell, the Fermi level lies between energy levels belonging to the two defects so that an electron exchange occurs, leading to Coulombic attraction).

So far we have shown that Fe_{Li}'s in b-axes channels are likely to have a V_{Li} adjacent to them along the same channel. In order to explain the aggregation of Fe_{Li}'s only in select few b-axis channels, we now consider the fact that Li diffusion in olivine $LiFePO_4$ is one-dimensional along the b-axis channels. We have verified, using the nudged-elastic-band method [13], that the migration barrier for a V_{Li} along the b-axis channel is in fact lowest by far, with

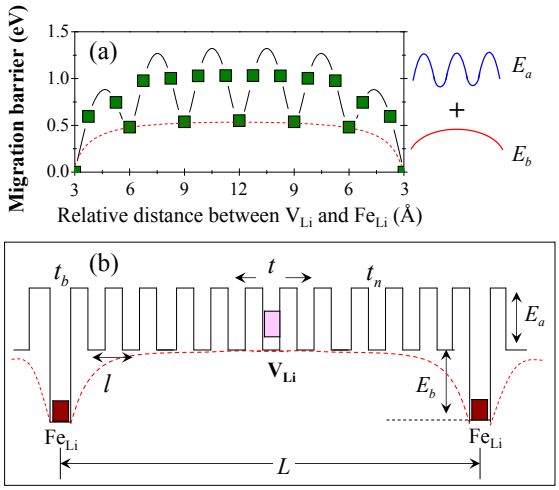

FIG. 2: (Color online) (a) Energy landscape for a V_{Li} shuttling between two Fe_{Li}'s in a b-axis channel combining migration barrier and binding energy variation. (b) Schematic version of the same figure, defining a one dimensional random walk with absorbing end points. The symbols are defined in the text.

a value of 0.5 eV, in good agreement with prior results [8, 14]. The key point now is what happens when more than one Fe_{Li} are present in the same channel: a V_{Li} that happens to be between two Fe_{Li}'s in the same b-axis channel can shuttle between the two end-points of the segment, possibly bind at either end, then be released again and shuttle until it gets bound again to one of the end points. The potential seen by a V_{Li} in such a segment is shown in Fig. 2(a). Intuitively, we can expect that in shorter segments the V_{Li} will bind more frequently and overall spend more time being bound than free. Segregation of the Fe_{Li} in just a few b-axis channels produces shorter segments between adjacent Fe_{Li} and hence more time when V_{Li}'s are bound. This is the source of energy lowering that produces the observed segregation. It is clearly a feature of the one-dimensional nature of Li diffusion.

In order to quantify the above effect, we map the shuttling of the V_{Li} between two Fe_{Li}'s on a one-dimensional random walk [19, 20] as illustrated in Fig. 2(b). We define the *energy lowering* arising from a single segment containing a single V_{Li} to be proportional to the ratio of the time t_b that a V_{Li} spends bound to an end-point Fe_{Li} to the sum of t_b and the time t that a V_{Li} spends shuttling prior to being bound:

$$E = \frac{t_b}{t + t_b} E_b. \tag{1}$$

In the case of an absorbing boundary, t is approximately given by [19–21]

$$t \simeq \frac{N^2}{4} t_n = \frac{L^2}{4l^2} t_n, \tag{2}$$

where t_n is the time of a single migration jump of length l as shown in Fig. 2(b). According to transition state theory [22],

$$t_n = \nu^{-1} \exp(\frac{E_a}{k_B T}), \tag{3}$$

where ν is the characteristic attempt frequency and E_a is the V_{Li} migration energy. Near the boundary, V_{Li} is attracted and can be bound with binding energy E_b, whereby t_b is given by

$$t_b = \nu^{-1} \exp(\frac{E_a + |E_b|}{k_B T}) = \exp(\frac{|E_b|}{k_B T}) t_n. \tag{4}$$

We then have

$$\frac{t}{t_b} = \frac{L^2}{4l^2 \exp(\frac{|E_b|}{k_B T})}. \tag{5}$$

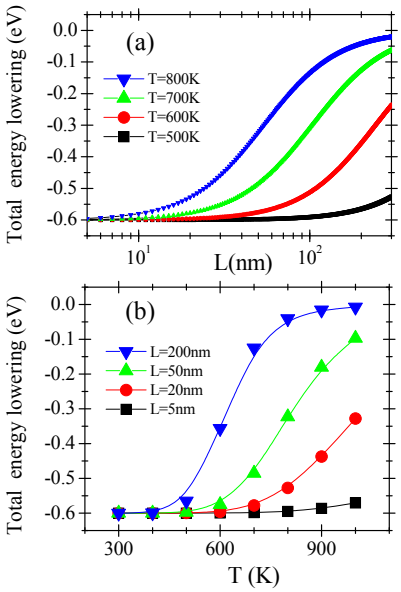

FIG. 3: (Color online) Total energy lowering a) as a function of separation L between Fe_{Li}'s and b) as a function of temperature T.

Consequently, the total energy lowering E can be expressed as a function of the distance L between two Fe_{Li} defects:

$$E(L) = \frac{E_b}{1 + (\frac{L}{b_0})^2 \exp(-\frac{|E_b|}{k_B T})}. \quad (6)$$

Here b_0 is the interatomic spacing of Li atoms along the b-axis, k_B is the Boltzmann constant, and T is the temperature at which the diffusion of V_{Li} occurs (synthesis temperature). The energy lowering E(L) is plotted in Fig. 3 as a function of L and as a function of T. Fig. 3(a) shows that for each temperature at which the synthesis occurs, shorter segments mean lower energy, which is the driving force of the observed segregation of Fe_{Li}'s in only a few b-axis channels. The process is of course ultimately limited by kinetic constraints. The message of the figure, however, is that a lower synthesis temperature favors the desirable segregation, but a lower temperature also means that kinetic constraints are more effective in limiting the segregation. Extended annealing at a relatively low temperature, smaller than 600 K, can be most effective in producing increased segregation. These results explain why Fe_{Li}'s are present if the samples are synthesized at temperatures lower than 200°C [23, 24], or when the samples are annealed at 600°C [12], whereas Fe_{Li}s are scarcely observed when the samples are annealed at 800°C [12].

So far we considered only the case of individual segments with a single V_{Li} between two Fe_{Li}'s. The case of more than one V_{Li} in a segment can in principle be treated but the results are not expected to change significantly as V_{Li}'s are indistinguishable. When we consider multiple segments, we recognize the possibility that V_{Li}-Fe_{Li}-V_{Li} complexes can form, as shown in Fig. 4. Clearly, the shorter the segments are, which lowers the energy of the system, the higher the probability of forming these complexes. We will now present experimental evidence that such complexes in fact exist.

To investigate the presence of V_{Li}-Fe_{Li}-V_{Li} complexes, we obtained atomic-resolution EELS in a $LiFePO_4$ sample using an aberration-corrected Nion UltraSTEM [25] at 100 kV operating voltage. The convergence semi-angle for the incident probe was 31 mrad, with an EELS collection semi-angle of 48 mrad, both of which are confirmed to effectively eliminate any effects of crystal anisotropy for bulk Fe. An acquisition time of 0.2 seconds per spectrum and an energy dispersion of 1 eV per channel was used. The Fe L-edge spectra (background subtracted) shown in Fig. 4. are the result of the sum of 8 and 10 individual spectrum for Fe_{Li} and a $LiFePO_4$ bulk, respectively. It is well accepted that the ratio between the L_3 and L_2 peak can be used as an indication of the oxidation state, with larger L_3/L_2 ratio corresponding to higher Fe valence.[26]. We find that the Fe L_3/L_2 ratio (calculated using the second derivative method [27]) for the Fe_{Li} is 18 % larger than that for the Fe in the bulk position. This qualitatively indicates that the oxidation state of Fe at the antisite position is higher than the average oxidation state of Fe in the bulk $LiFePO_4$ material (i.e., +2). Indeed, the nominal Fe oxidation state in Fe_{Li} is +1, in Fe_{Li}-V_{Li} it is +2, and in V_{Li}-Fe_{Li}-V_{Li} it is +3, whereby the presence of V_{Li}-Fe_{Li}-V_{Li} accounts for the observed Fe oxidation state higher than +2. A comparison

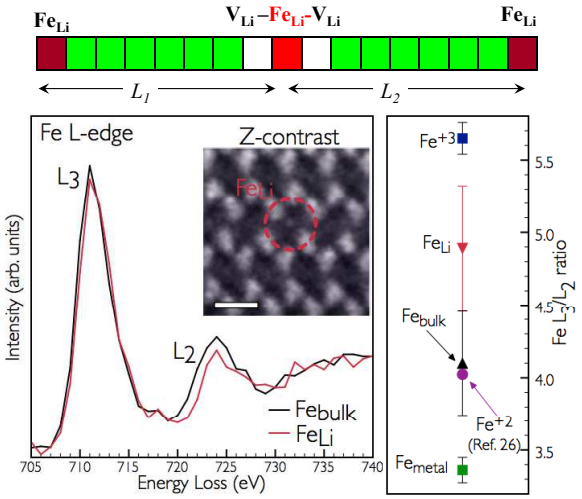

FIG. 4: (Color online) Top: Schematic figure of probable configuration of Fe_{Li} with higher Fe oxidation state. Bottom: (Left) EELS data from Fe_{Li} (in red circle in the inset) and of Fe in bulk positions in $LiFePO_4$. The inset shows an atomically-resolved Z-contrast image of $LiFePO_4$ oriented along the b-axis. Scale bar is 0.5 nm.(Right) Fe L_3/L_2 ratios for Fe_{Li} (red triangle) and Fe_{bulk} (black triangle) sites of $LiFePO_4$ compared with different iron compounds. Fe^{+3} and Fe_{metal} correspond to spectra obtained for α-Fe_2O_3 and metallic iron thin film, respectively. The data point shown as a purple circle corresponds to the Fe L_3/L_2 ratio of the FeO spectra, i.e. Fe^{+2}, presented in Ref. 26 and calculated using the second derivative method of Ref. 27. The data point is shown only for comparison purposes.

of the Fe L_3/L_2 ratios of Fe_{Li} site with respect to Fe_{bulk} site of $LiFePO_4$ and other iron compounds is also shown in Fig. 4.

In conclusion, we showed that the observed segregation of Fe_{Li}'s defects in selective b-channels is the result of an unusual energy-lowering mechanism that is a feature of the one-dimensional nature of the Li diffusion path. V_{Li}'s shuttle between Fe_{Li}'s defects and bind occasionally at the end-points along the b-channels. Segregation of Fe_{Li}'s in just a few channels results in shorter Fe_{Li}-Fe_{Li} separations, which induce longer binding times, lowering the system's energy. The analysis suggests temperatures for growth and/or annealing to optimize segregation and maximize Li diffusion.

We thank Dr. Nancy Dudney who supplied the $LiFePO_4$ sample for EELS measurement. This research was partially supported by the National Science Foundation under Grant No.DMR-0938330 (J-CI, WZ), by ORNL's Shared Research Equipment (SHaRE) User Facility, which is sponsored by the Office of Basic Energy Sciences, U.S. Department of Energy (J-CI) and the Office of Basic Energy Sciences, Materials Sciences and Engineering Division, U.S. Department of Energy (SJP, JL,STP), DOE grant DE-FG02-09ER46554 (STP), and by the McMinn Endowment (STP) at Vanderbilt University. This research used resources of the National Energy Research Scientific Computing Center, which is supported by the Office of Science of the U.S. Department of Energy under Contract No.DE-AC02-05CH11231.

[1] A. K. Padhi *et al.*, J. Electrochem. Soc. **144**, 1188 (1997).
[2] B. L. Ellis *et al.*, Chem. Mater. **22**, 691 (2010).
[3] S. Nishimura *et al.*, Nat. Mater. **7**, 707 (2008).
[4] C. Quyang *et al.*, Phys. Rev. B **69**, 10403 (2004).
[5] S.-Y. Chung *et al.*, Angew. Chem., Int. Ed. **48**, 543 (2009).
[6] G. Kresse *et al.*, Comput. Mater. Sci. **6**, 15 (1996).
[7] F. Zhou *et al.*, Electrochem. Commun. **6**, 1144 (2004).
[8] M. S. Islam *et al.*, Chem. Mater. **17**, 5085 (2005).
[9] C. A. Fisher *et al.*, Chem. Mater. **20**, 5907 (2008).
[10] D. B. Laks *et al.*, Phys. Rev. B **45**, 10965 (1992).
[11] W. Luo *et al.*, Phys. Rev. Lett. **99**, 036402 (2007).
[12] S.-Y. Chung *et al.*, Phys. Rev. Lett. **100**, 125502 (2008).
[13] G. Mills *et al.*, Surf. Sci. **324**, 305 (1995).

[14] D. Morgan *et al.*, Eeltrochem. Solid-State Lett. **7**, A30 (2004).
[15] P. Axmann *et al.*, Chem. Mater. **21**, 1636 (2009).
[16] K. C Smith *et al.*, Phys. Rev. B **82**, 134109 (2010).
[17] G. R. Gardiner *et al.*, Chem. Mater. **22**, 1242 (2010).
[18] R. Malik *et al.*, Nano Lett. **10**, 4123 (2010).
[19] M. A El-Shehawey, J. Phys. A:Math. Gen. **33**, 9005 (2000).
[20] M. A El-Shehawey, J. Matrix Anal. Appl. **30**, 497 (2008).
[21] The full expression is $t = (\frac{N^2}{4} + N\frac{1-\beta}{\beta})t_n$, where β, the absorption probability is given by $\beta \simeq 1 - \frac{t_n}{t_b}$ =1-exp($-\frac{|\mathrm{E_b}|}{\mathrm{k_B T}}$) $\simeq 1$
[22] G. H. Vineyard, J. Phys. Chem. Solids. **3**, 121 (1957).
[23] J. Chen *et al.*, Electrochem. Commun. **8**, 855 (2006).
[24] S. Yang *et al.*, Electrochem. Commun. **4**, 239 (2002).
[25] O.L. Krivanek *et al.*, Ultramicroscopy **110**, 935 (2010).
[26] C. Colliex *et al.*, Phys. Rev. B **44**, 11402 (1991).
[27] G.A. Botton *et al.*, J. Electron Microsc. **180**, 211 (1995).